

# Shock structures and instabilities formed in an underexpanded jet impinging on to cylindrical sections

N. Mason-Smith · D. Edgington-Mitchell ·  
N. A. Buchmann · D. R. Honnery · J. Soria

Received: 29 October 2013 / Revised: 11 February 2015 / Accepted: 25 February 2015 / Published online: 12 March 2015  
© Springer-Verlag Berlin Heidelberg 2015

**Abstract** Schlieren visualisations are used to investigate the influence of cylindrical surface curvature on both the time-invariant and oscillatory behaviour of the shock structures within underexpanded jets impinging on to a surface. At moderate standoff distances ( $\frac{h}{d} < 5$ ), the impingement surface curvature affects the temporal behaviour of the flow significantly, but with only slight variations in the time-invariant structure. A convex surface curvature constrains flapping oscillations to a single plane, the normal of which is parallel to the cylinder axis; the oscillation frequency is largely unaffected. For the standoff distances and nozzle pressure ratios studied, concave surface curvature suppresses the formation of impingement tones. A mechanism is proposed whereby entrainment of the recirculated wall jet flow alters the shear layer receptivity to acoustic disturbances, breaking the acoustic feedback loop that drives the jet oscillations.

**Keywords** Aeroacoustics · Schlieren · Impinging jet

## 1 Introduction

The underexpanded impinging jet is a shock-containing flow, the structure of which is known to depend on the plate standoff distance and the nozzle pressure ratio:

---

Communicated by F. Seiler.

N. Mason-Smith (✉) · D. Edgington-Mitchell · N. A. Buchmann ·  
D. R. Honnery · J. Soria  
Monash University, Melbourne, Vic, Australia  
e-mail: nick.masonsmith@gmail.com

D. Edgington-Mitchell  
e-mail: daniel.m.mitchell@gmail.com

$$\text{NPR} = \frac{p_0}{p_a}, \quad (1)$$

where  $p_0$  is the total pressure in the plenum, and  $p_a$  is the ambient pressure [14]. The mean shock structure is characterised by a series of shocks and expansion waves. A feature distinguishing underexpanded impinging from free jets is the plate shock, which is a normal shock above the impingement surface through which the flow decelerates to subsonic speeds and is radially redirected into the wall jet. Figure 1 shows the structure of the underexpanded impinging jet. The presence of a recirculation region and the size and shape of the shocks are functions of nozzle pressure ratio and standoff distance [8].

Early studies into impinging jets focused on mean jet structure and the pressure exerted on the impingement plate [4]. Mean flow features of supersonic impinging jets, particularly the shock cell structure, were the focus of previous studies by the group of Hunt [2, 9, 12]. Flows on to inclined impingement plates were also studied [13].

The supersonic impinging jet is characterized by large-scale oscillatory motion of both the jet boundary and the embedded shock structure. An acoustic feedback loop drives this oscillatory process and operates as follows: instabilities in the shear layer at the nozzle exit grow into large vortices, which convect downstream and disturb the jet shocks. Shock–vortex interaction, particularly in the standoff region, produces shock movements that alter the flow characteristics. Pulsatile motion of the wall jet [8] gives rise to high-intensity acoustic waves which travel upstream and perturb the shear layer, closing the feedback loop. Phase-locked [7] and time-resolved [14] visualisations have demonstrated the presence of this feedback loop. The acoustic feedback loop also occurs in impinging jet flows on to inclined plates [19].

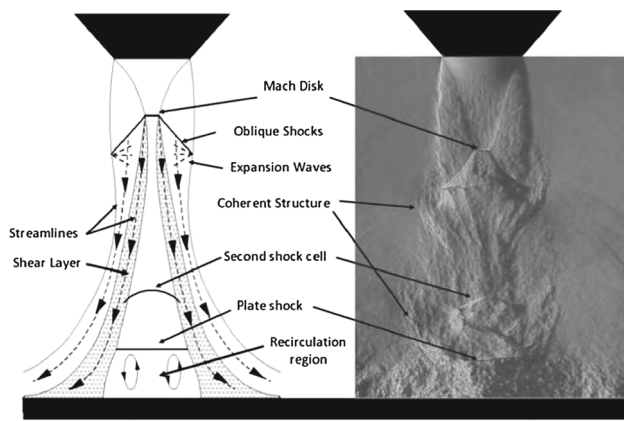


**Fig. 1** Schematic of the underexpanded impinging jet, adapted from Mitchell et al. [14]

Early investigators observed oscillations in the supersonic jet [20] and classified these oscillations as symmetrical and asymmetrical [16]. In the symmetrical mode, large toroidal vortices (also known as ring vortices) span the jet. Asymmetric oscillations can be either helical or flapping, and the flapping motion is the combined effect of two counterrotating helical oscillations [20]. The helical oscillation is also known as the spiral mode, and the flapping oscillation is also known as sinuous [16]. These oscillations are associated with ‘impingement tones’, which are high-intensity sounds of discrete frequency. An impinging jet which produces broadband noise with no discrete peaks is said to be in a ‘zone of silence’, and does not display large-scale oscillations [7].

The frequency and amplitude of impingement tones is of practical interest. Powell’s model enabled the prediction of impingement tone frequency in supersonic jets [16] and requires the convective speed of jet disturbances to determine the impingement tone frequency. Powell’s feedback formula is given by

$$\frac{N + p}{f} = \int_0^{h'} \frac{dh}{c_0} + \int_0^{h'} \frac{dh}{u_{\text{con}}}, \quad (2)$$

where  $N$  is the number of jet disturbances per cycle,  $p$  the combined phase lag at the sound source and the nozzle,  $f$  the frequency,  $h'$  the distance from the nozzle to the sound source,  $c_0$  the ambient speed of sound and  $u_{\text{con}}$  the convective speed of jet disturbances [16]. Experiments by Krothapalli et al. [10] showed that this speed could be obtained by particle image velocimetry, and good agreement was found between the predicted and experimentally observed impingement tone frequency.

The discovery that shear layer thickness plays a crucial role in acoustically sensitive jets dates back to Rayleigh [17]. Altering the initial shear layer can suppress impingement tones and jet oscillations, and this understanding is the basis for flow control techniques. For example, microjet control

of supersonic impinging jets works by thickening the initial shear layer, reducing its receptivity to acoustic disturbance [1]. The use of microjets has been shown to considerably reduce impingement tones and jet oscillations in laboratory applications, although their success has been found to depend on the type of instability in the jet [11].

Research to date has generally focused on planar impingement geometries. What is not well understood is the effect of impingement surface curvature on the shock structure of the jet. Furthermore, it is not known how the impingement surface curvature affects the instabilities formed in the supersonic jet flow. Previous research on cylindrical surface impingement was constrained to low Reynolds number subsonic jets [3]. Noted in the research is the absence of coherent ring vortex formation when a concave cylindrical impingement surface is used.

This paper presents experiments using schlieren to visualise the shock structures and instabilities formed by an underexpanded jet impinging on convex and concave half-cylinders, and a flat plate for comparison. Mean and RMS schlieren images are used to characterise the effect of surface curvature on the shock structure at several pressure ratios. The effects of cylindrical surface curvature on the formation of impingement tones and jet oscillations are explored, and mechanisms proposed for the observed results.

## 2 Experimental methodology

### 2.1 Supersonic jet rig

The experiments were undertaken in the Laboratory for Turbulence Research in Aerospace and Combustion Supersonic Jet Facility; a schematic of the jet facility is shown in Fig. 2. Compressed air issues from a converging nozzle with exit diameter 15 mm. Continuous operation is possible for nozzle pressure ratios less than 5. The nozzle pressure ratio is maintained through the use of a Fairchild 100 High Flow pressure regulator, with a delivery pressure stability of <0.007 bar per 7 bar of upstream variation, and an RS-461 pressure transducer capable of measuring up to 10 bar with uncertainty of  $\pm 0.25\%$ . Flow conditioning is achieved through the use of honeycombs and mesh screens in the plenum chamber located upstream of the jet.

### 2.2 Impingement plates

Convex and concave aluminium half-cylinder impingement plates are used, each with a radius of curvature of 37.5 mm (2.5 nozzle diameters) and a length of 115 mm. The plates are mounted to a rig capable of precise positioning of the plate relative to the nozzle. The flow on to the convex cylinder is visualised in the  $xy$  and  $xz$  planes (as per Fig. 3), these

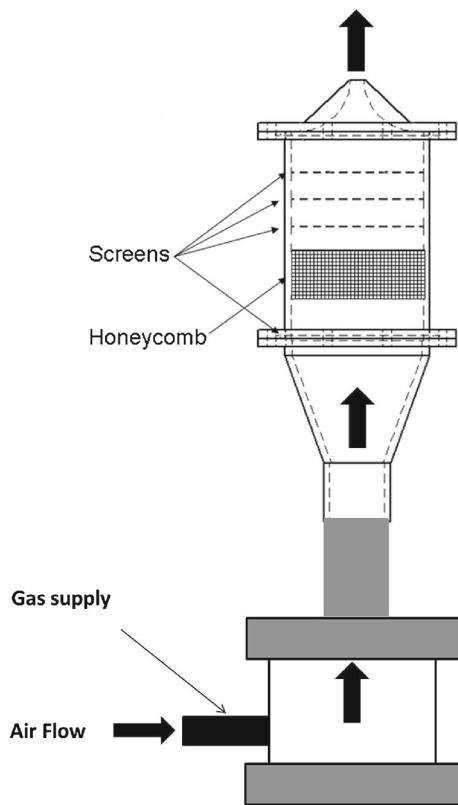


**Fig. 2** The supersonic jet apparatus, adapted from Mitchell et al. [15]

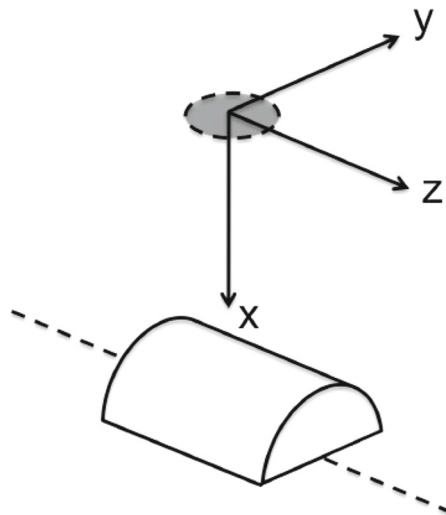


**Fig. 3** Coordinate system for the presented results. The origin is located at the *centre* of the nozzle exit, which is indicated by the shaded *circular* region. The *x*-axis lies along the nozzle *centreline*, and the *z*-axis is parallel to the cylinder axis for both the convex and concave configurations. As the flat plate is symmetric about the *x*-axis, the *y* and *z* terms are substituted with a single *r* coordinate

are termed on-axis and off-axis, respectively. The plates are all greater than two nozzle diameters across, and as such may be considered large plates [7]. The plate was positioned

precisely using gauge blocks between the nozzle lip and the geometric impingement point, and the measured standoff distance  $h$  is used in the results.

### 2.3 Shadowgraph and schlieren apparatus

A Toepler Z-type schlieren arrangement was used to visualise density gradients in the impinging jets. A Phlatlight CBT-120 LED was used as the light source; a monochromatic LED light source for schlieren produces images with less chromatic aberration than a typical flash-lit schlieren image and permits the collection of many exposures in quick succession [22]. Two 200 mm-diameter parabolic mirrors with focal lengths of 2 m were used to collimate and focus the light. A PCO Dimax camera was used to collect images with 12-bit radiometric resolution at a magnification of 20 pixel/mm. One thousand instantaneous images were collected for each plate-height-NPR configuration studied; image integration time was 1.28  $\mu$ s which is short enough to sharply visualise dynamic flow features. Axial density gradients were visualised by positioning the knife edge perpendicular to the axial flow direction, and a light source cutoff of 70% was used to enable visualisation of the density gradients while retaining measuring range.

### 2.4 Acoustic measurements

A G.R.A.S. 46BE 1/4" freefield microphone was used to measure the sound generated by the impinging jet. The microphone was aimed at the impingement point and positioned in the nozzle lip plane at a distance of 16 nozzle diameters from the impingement point. The preamplified signal was then recorded with a National Instruments USB-6212 16-bit DAQ and Labview software. A sampling rate of 200 kHz was used, and the Nyquist cutoff frequency was 100 kHz. 500,000 samples were taken with the microphone and a sliding Hann window was used in the FFT to produce the spectra. For this study, an impingement tone is defined as a peak 10 dB or greater above the local sound pressure level. Acoustic results are presented in terms of the Strouhal number, a dimensionless number that relates the acoustic frequency to the velocity of the jet:

$$St_{\text{nozzle}} = \frac{fd}{u_e}, \quad (3)$$

where  $u_e$  is the velocity at the jet nozzle exit plane,  $d$  is the nozzle exit diameter and  $f$  is the frequency. Previous studies [6–8, 16] into the acoustics of impinging jets have characterised impingement tones by their acoustic wavelength normalised by the jet diameter ( $\lambda/d$ ). For a cold choked jet where the nozzle exit velocity is equal to the ambient speed of sound, the Strouhal number is the reciprocal of  $\lambda/d$ . In this case, the exit velocity is determined from particle image

velocimetry results to be 310 m/s [5]. To compare the presented results with prior studies,

$$\frac{\lambda}{d} = \frac{c_a}{St.u_e} \quad (4)$$

where  $c_a$  is the ambient speed of sound.

### 3 Results and discussion

#### 3.1 Mean shock structures

The mean shock structure is obtained by ensemble averaging 1000 instantaneous schlieren images for each plate-height-NPR case. Figure 4 shows the mean shock structures at NPR 3.0 (left) and NPR 3.4 (right) for the flat plate and convex plate on- and off-axis. Results for the concave plate are at NPR 2.9 (left) and NPR 3.4 (right). The knife edge is oriented such that regions of axial expansion appear darkened and axial compression appear brightened. These pressure ratio cases are presented because their acoustic spectra differ considerably, though the difference in pressure is quite small; consequently, the changes in shock structure are not solely attributable to the change in pressure ratio.

The axial position of the shock cells at NPR 3.0 appears similar for the flat plate and the convex plate from both views. A second shock cell is not clearly defined, suggesting that the shock structure is unsteady at this condition. Furthermore, the appearance of a strong dome shock in the first shock cell is indicative of collapse of the downstream shock structure [7]. The plate shock is visible on the convex plate viewed off-axis, and is upturned at its extremities. At this condition, it is possible that the impingement surface curvature results in the shock being ‘draped’ over the cylinder, and axial symmetry of the structures is not sustained. The plate shock is less clearly defined for the on-axis case and the flat plate.

The shock structure in the jet impinging on the concave plate appears stable, and two shock cells and a plate shock are clearly defined. As with the convex plate viewed off-axis, the plate shock is upturned at its extremities, suggesting that this shock structure does not remain axisymmetric. The axial position of the first shock cell is similar for the flat and convex plates, but is further downstream on the concave plate. A stable plate shock reduces flow velocity considerably before impact with the plate; the collapse of this shock results in an upstream forcing of the shock cells [8].

As the nozzle pressure ratio increases from 3.0 to 3.4, the spread of the jet after the first shock cell for the convex plate off-axis is significantly reduced. Conversely, the jet boundary widens and becomes more pronounced for the convex plate on-axis. Notably, the shock structures in the jet impinging on the convex plate appear more clearly defined viewed off-axis. The result of shock motion throughout the collection

sample is a smearing of the mean position; consequently, a more clearly defined shock is indicative of reduced motion. This difference in motion of the first shock cell suggests that the shock’s motion is not axisymmetric on the convex plate at NPR 3.4. To more clearly visualise the time-variant behaviour of the shocks, Fig. 5 presents the RMS of the schlieren images at the same conditions as Fig. 4.

The first shock cell in the jet impinging on the flat and convex plates at NPR 3.0 appears to remain axially stationary, but fluctuates between sharply angled oblique shocks and a dome-shaped shock. The plate shock on the convex plate is larger in size viewed off-axis. This suggests that the impingement surface curvature, though not considerably altering the first shock cell at NPR 3.0, does alter the structure of the plate shock. At NPR 3.4, the flat plate and the convex plate on-axis both display fluctuations of the first shock cell and downstream shocks. Viewed off-axis, the fluctuations of the first shock cell of the jet impinging on the convex plate appear localised, and as per the mean structure the jet spread is reduced. For the concave plate at both NPR 3.0 and NPR 3.4, the fluctuations appear localised to the shocks, suggesting an absence of coherent structures convecting along the jet.

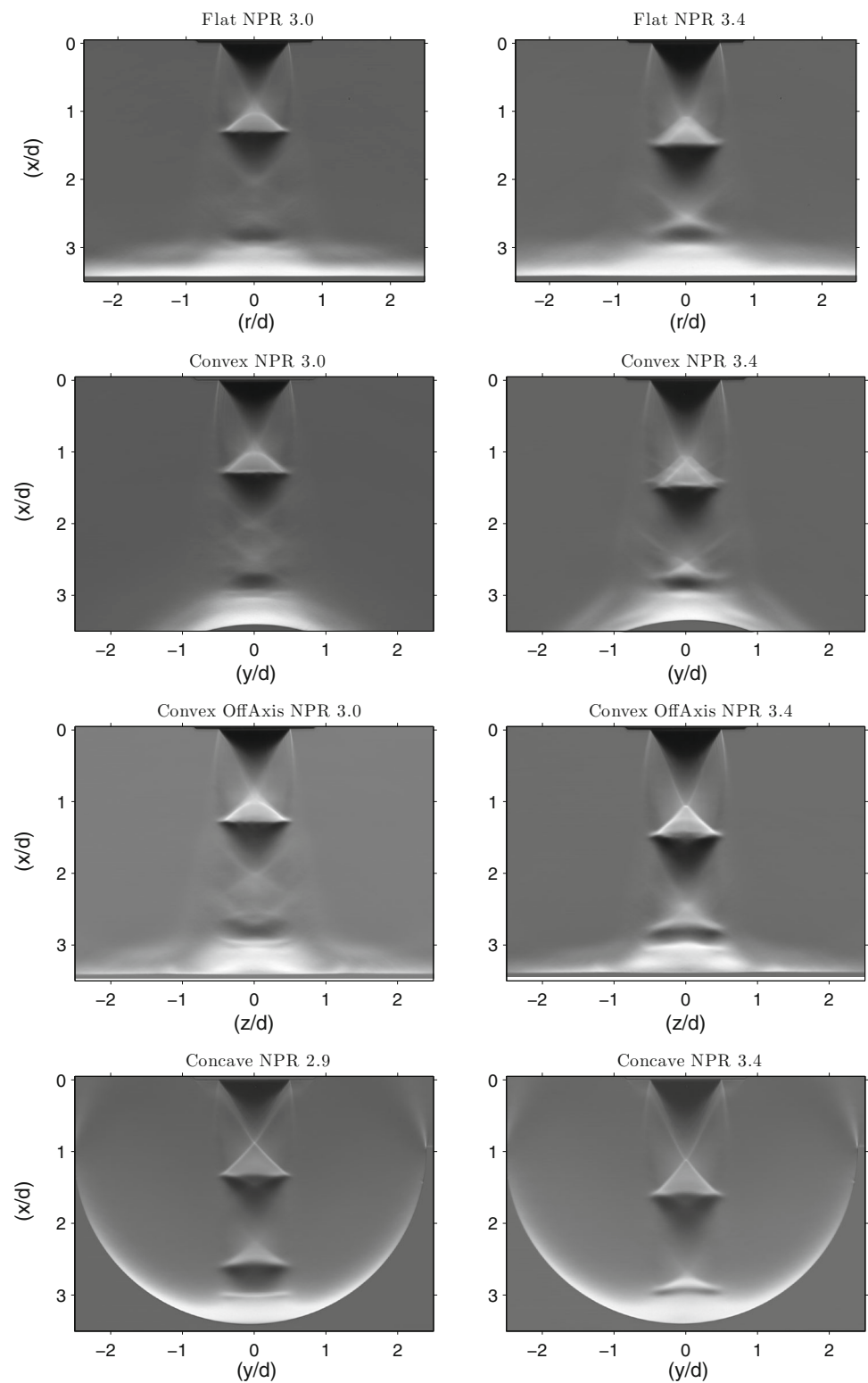
#### 3.2 Jet oscillations

Axisymmetric and asymmetric oscillations take place in underexpanded impinging jets [20]. Powell [16] found that the frequency of oscillation is largely invariant with nozzle pressure ratio at fixed heights, except where an additional disturbance per cycle is added. Impingement tones from acoustic measurements taken at  $\frac{h}{d} = 3.5$  are shown in Fig. 6. Though multiple tones are present at many cases, only the dominant fundamental impingement tone is presented. Tones are obtained from the power spectra via a peak finding algorithm with a threshold of 10 dB.

Several features are observable in the acoustic results. No impingement tones are produced on the concave plate for nozzle pressure ratios between 2.9 and 3.9; the presence of tones on the flat and convex plates at these pressure ratios suggests that this ‘zone of silence’ is not associated with the axial location of the plate in the free jet shock cell structure, unlike the zones of silence reported by Henderson [7]. Where tones are produced on the concave plate, the Strouhal number of the dominant fundamental impingement tone is very close to that of the tone produced on the flat plate. The flat and convex plate impingement tones both lie on lines of essentially invariant Strouhal number; the increase in Strouhal number with NPR is attributable to an increase in the convective speed of jet disturbances as per Powell’s model [Eq. (2)].

The acoustic results indicate the presence of jet oscillations, but do not provide insight into the type of jet oscillations taking place. Figure 7 shows instantaneous schlieren

**Fig. 4** Mean schlieren image at  $\frac{h}{d}$  3.5, NPR 3.0 (left column, except concave plate at NPR 2.9) and NPR 3.4 (right column). Each mean schlieren image is generated from 1000 instantaneous schlieren image samples



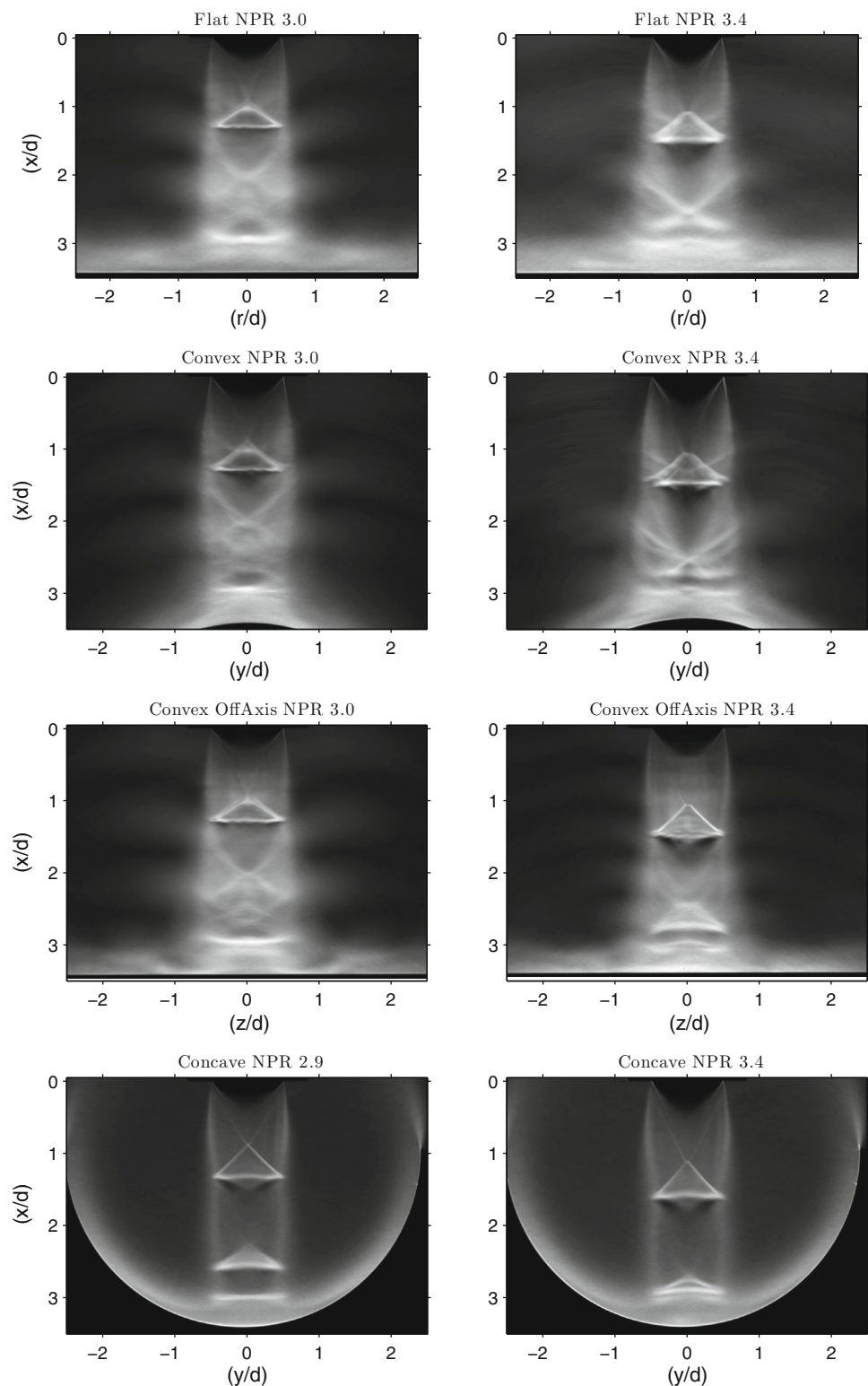
images of the jet impinging on the flat, convex and concave plates at NPR 3.0 and NPR 3.4 to visualise the flow features at these pressure ratios.

A distinct difference between the jet oscillation at NPR 3.0 and NPR 3.4 is observed for the convex and flat plates. Coher-

ent structures are identifiable in the image, as are acoustic waves surrounding the jet. The instantaneous images at NPR 3.0 show coherent structures that are symmetrical about the jet centreline; conversely at NPR 3.4, both the coherent structures and acoustic waves appear to be of opposite phase on



**Fig. 5** RMS schlieren images showing the oscillations of the jet structure at  $\frac{h}{d}$  3.5, NPR 3.0 (left column, except concave plate at NPR 2.9) and NPR 3.4 (right column). Each RMS schlieren image is generated from 1000 instantaneous schlieren image samples



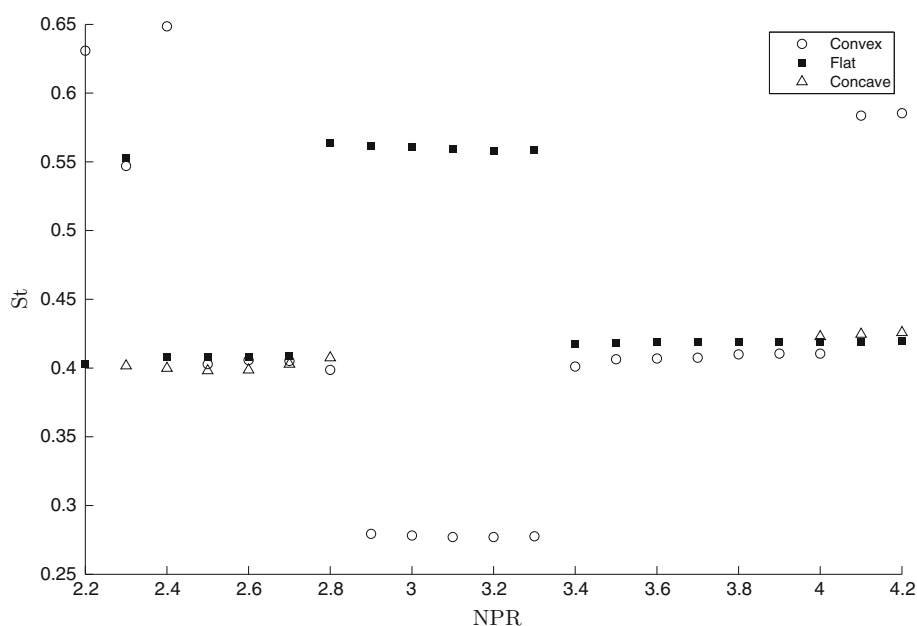
either side of the jet centreline. For the concave cases presented, neither acoustic waves nor coherent structures are discernible, which is attributable to the absence of impingement tones at this case.

As a means to characterise the instability mode, the two-point correlation function is applied to the instantaneous

schlieren images. The correlation  $R$  of two discrete random variables  $x$  and  $y$  is given by

$$R_{x,y} = \frac{\sum_{i=1}^n ((x_i - \mu_x)(y_i - \mu_y))}{n\sigma_x\sigma_y}, \quad (5)$$

**Fig. 6** Impingement tone Strouhal numbers vs nozzle pressure ratio,  $\frac{h}{d} = 3.5$



where  $\mu_k$  and  $\sigma_k$  are the mean and standard deviation of variable  $k$ , respectively,  $n$  is the number of samples for each variable, and  $k_i$  denotes the  $i^{\text{th}}$  sample of variable  $k$ .

Applying this to a set of visualisation images yields a useful image depicting spatial relationships in the flow, despite the relatively qualitative data from the schlieren images [22]. Two-point correlation results are presented in Fig. 8, with the reference position  $(x, y)$  indicated by the crossing of the dashed lines. The point of interest is located in the initial shear layer, with the exception of the convex cylinder off-axis case at NPR 3.4 as the jet disturbances do not extend to the visible shear layer (as per Fig. 9, right). Care must be taken in interpreting the two-point correlation images, as the variable being correlated is the path-integrated density gradient and not a fluid property; here, the two-point correlation is used as a visualisation technique.

A change in instability type is observable with the change in pressure ratio. Of note is the symmetrical appearance of the disturbances at NPR 3.0, and a consistency in the sign of the correlation on opposite sides of the jet, suggesting the presence of an axisymmetric mode. For the convex case at NPR 3.4, a marked difference is apparent in the correlation image for the on-axis and off-axis views. Viewed off-axis, the correlation image remains symmetrical about the jet centreline, whereas a distinct asymmetry is observable for the on-axis case. These results suggest that a flapping oscillation occurs at this pressure ratio and height, and the flapping plane is orthogonal to the cylinder axis. This contrasts with flapping oscillations in underexpanded free jets, where the flapping plane does not necessarily remain stationary [21].

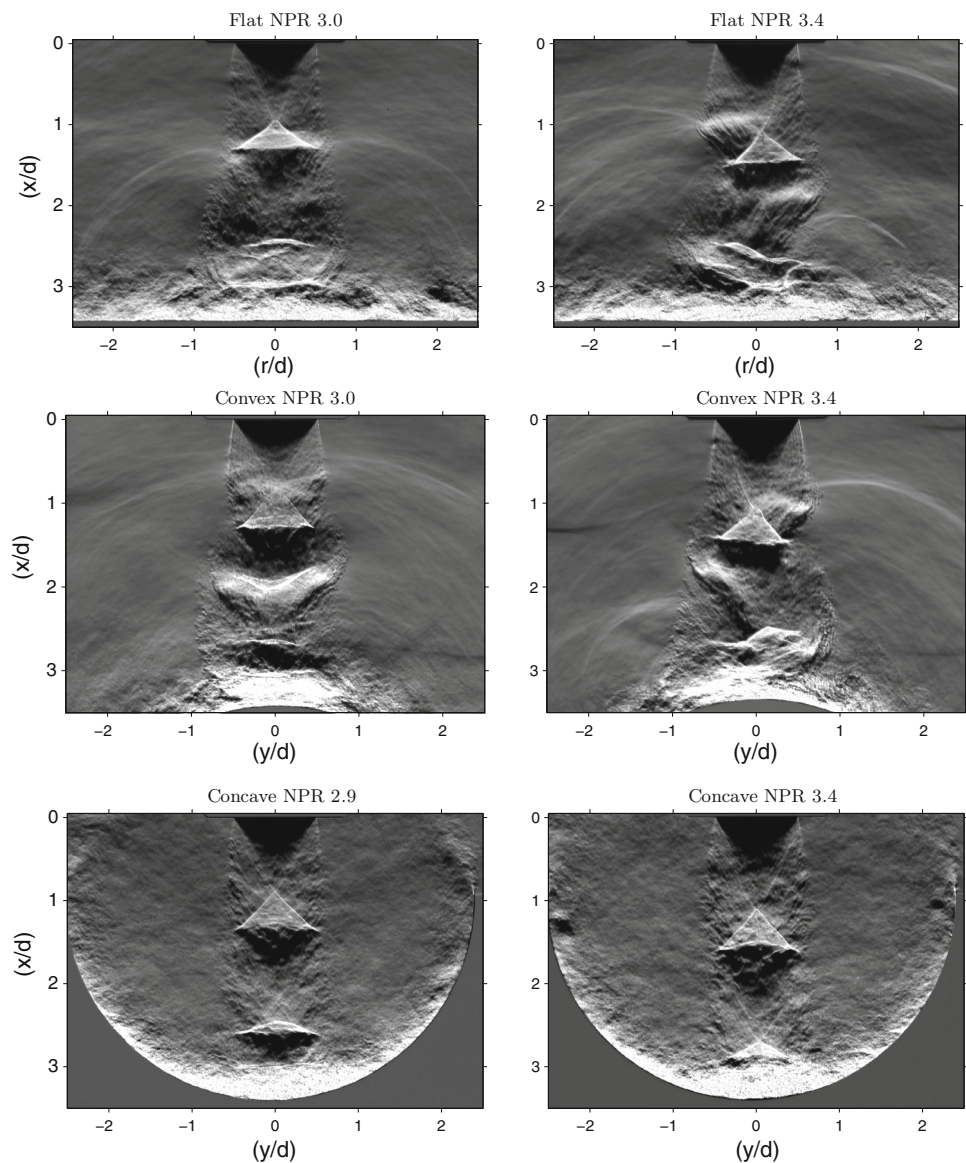
For the underexpanded jet impinging on to a flat plate, the flapping plane has no preferential orientation and precesses. The appearance of the jet and acoustic field depends on the

orientation of the jet flapping plane relative to the image plane. With the flapping plane parallel to the image plane, the jet disturbances are visible in the shear layer and the asymmetry of the jet is visible (Fig. 7, right). When the flapping plane is orthogonal to the image plane, the jet disturbances are seen as symmetrical bands across the jet (Fig. 9). Throughout the image set, the jet is visualised at many different orientations between these two extremities. As the relationship between the visualised acoustic field and jet disturbances is a function of the angle of the flapping plane relative to the image plane, attempts to perform the two-point correlation for the flapping oscillation on the flat plate produce a weak correlation image. Cylindrical surface curvature appears not to influence the type of instability, but prevents the precession as observed on the flat plate. This may be the result of preferential destabilisation of the shock, leading to altered feedback to the nozzle.

### 3.3 Suppression of oscillations on the concave plate

A weak impingement tone is produced on the concave plate at pressure ratios where very high amplitude tones are produced on the convex and flat plates (Fig. 10). At a nozzle pressure ratio of 3.4, impingement tones of high amplitude at Strouhal numbers 0.418 and 0.401 are present in the acoustic power spectra for the flat plate and convex plate, respectively (Fig. 10). At this same condition, a weaker impingement tone is present at a Strouhal number of 0.419 for the concave plate, and the jet appears undisturbed from its mean structure (Fig. 5, bottom right). These results suggest that the concave surface curvature disrupts the operation of the feedback mechanism. As all stages of the feedback loop are necessary for self-sustained oscillation, a range of mechanisms exist

**Fig. 7** Instantaneous schlieren images of an underexpanded jet impinging on to a flat plate, convex cylinder and concave half cylinder at  $\frac{h}{d}$  3.5, NPR 3.0 (left column) and NPR 3.4 (right column)



by which the cycle may be disrupted and impingement tones suppressed. Zones of silence were reported in the results of Henderson [8] and found to depend on the position of the plate in the structure of the corresponding free jet. The presence of tones for both the convex and flat plate cases suggests that it is not the position of the concave plate that causes the suppression of tones.

Reflected acoustic waves can destructively interfere at the initial shear layer with the acoustic waves emitted by the jet [6]. This is a mechanism of impingement tone suppression, but it does not appear to explain the weaker tone on the concave plate. Experiments by Henderson and Powell [6] examined the role of acoustic feedback in the generation of impingement tones by installing a reflector at the nozzle exit. At reflector positions where high-amplitude large plate tones were suppressed, tones of previously lower amplitude were

amplified [6]. The acoustic power spectrum for the concave plate in Fig. 10 (right) displays no peaks of higher amplitude than the power spectra for the convex and flat plates at the same height and NPR. If acoustic reflection were the mechanism by which the concave plate suppresses impingement tones, an amplified tone at another Strouhal number would be expected. Given the absence of such a tone, this is an unlikely explanation for the observed phenomenon.

Another mechanism by which impingement tones may be suppressed is the alteration of the shear layer's receptivity to acoustic excitation. Microjets have been shown to suppress impingement tones, and the mechanisms of tone suppression are a thickening of the initial shear layer and increased streamwise vorticity in the jet [1]. Experiments on low-speed impinging jets found a suppression of large ring vortices when a concave cylindrical impingement surface curvature



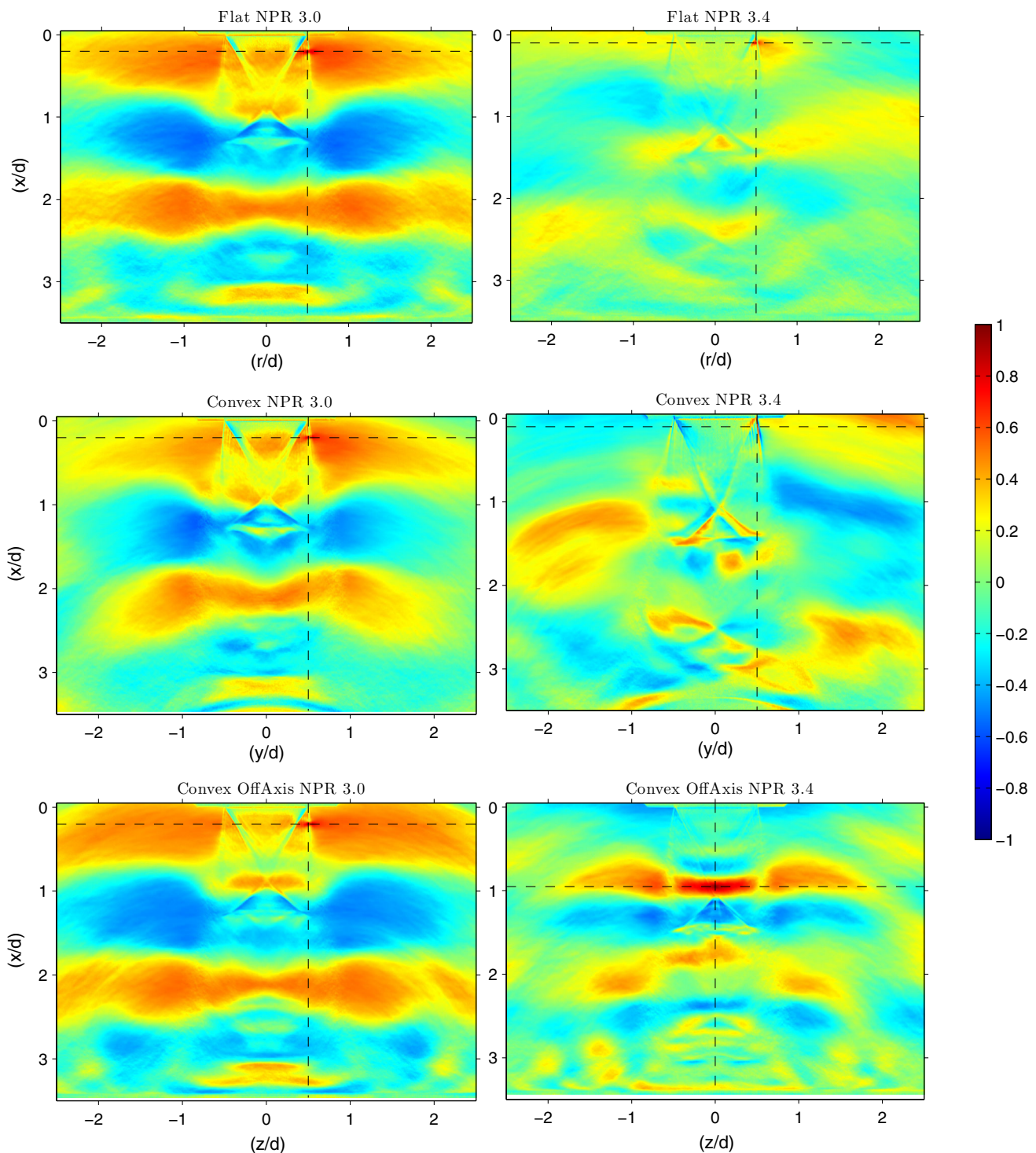


**Fig. 8** Two-point correlation results on flat and convex plates, NPR 3.0 (*left column*) and NPR 3.4 (*right column*) at  $\frac{h}{d} = 3.5$ . Each correlation image is generated from 1000 instantaneous schlieren images. Pixels of interest are located in the jet shear layer and are indicated by *dashed lines*

was used [3], which was attributed to recirculation of the wall jet into the initial shear layer.

The concave impingement surface curvature directs the turbulent wall jet into the jet entrainment field. The recirculation of the exhaust flow may lead to an increase in dis-

turbances of the shear layer that are less impulsive than the acoustic feedback, and an increase in mixing in the shear layer. This increase in mixing is similar to the effect produced by nozzle tabs, which suppresses screech in free jets [18]. Though the mechanisms are different, the effect of the

**Fig. 9** Instantaneous schlieren photographs of underexpanded jets impinging on a flat plate (left) and a convex cylinder, viewed off-axis (right) at  $\frac{h}{d} = 3.5$

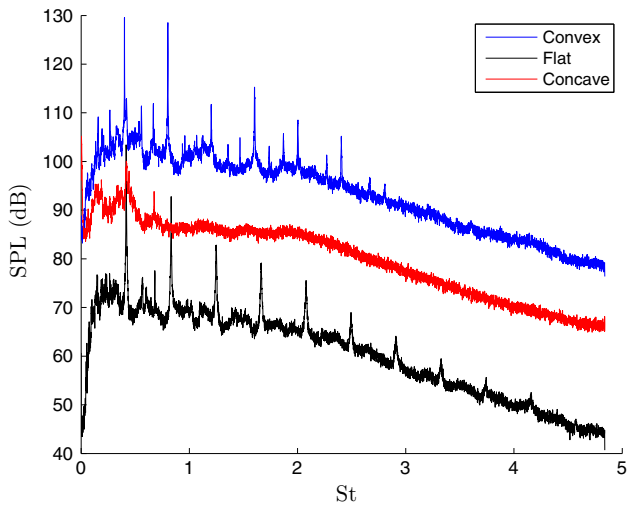
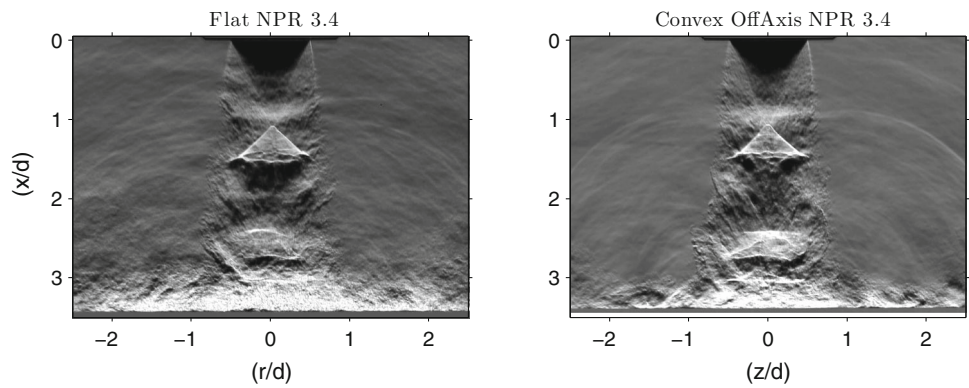


**Fig. 10** Power spectrum of acoustic signal generated by impinging jet at  $\frac{h}{d} = 3.5$ , NPR 3.4. The sound pressure level for the concave and flat plates have been displaced downwards by 10 and 20 dB, respectively, for clarity of comparison

concave impingement surface curvature may similarly result in increased mixing, a thickening of the shear layer and hence a reduction in its receptivity, thereby disrupting the acoustic feedback process. Figure 11 shows instantaneous schlieren images of the jet shear layer and close entrain-

ment field for the impinging jet on the concave and convex plates.

The convex plate directs the wall jet away from the nozzle; consequently, the variation in image intensity in the entrainment region (Fig. 11, right) is the product of acoustic emission and pressure variations in the entrained fluid. The variations are predominantly seen as peaks and troughs of waves travelling in the axial direction. For the concave case, the schlieren image of the entrainment field appears much more varied and is particularly strong at the mixing layer where the wall jet leaves the plate (Fig. 7, bottom). The variation appears to be more random, with little coherence in either the axial or radial direction. The additional fluctuation for the concave case is expected to be the result of vortical structures in the recirculated wall jet in the entrainment region.

To generalise this result from instantaneous images, the coefficient of variation ( $\frac{\sigma}{\mu}$ ) of a region of interest in the entrainment region (indicated in Fig. 11) is compared for the concave and convex cases through the image set. The mean and standard deviation are calculated from the collected intensity values in the region of interest for 1000 images; this corresponds to approximately 80 million samples. The selected height and pressure ratio for the two plates is in a ‘zone of silence’ [7] to ensure that high-amplitude impingement tones do not significantly affect the comparison. To illustrate this point, instantaneous images showing the pres-

**Fig. 11** Instantaneous schlieren image of entrainment field and initial shear layer of the impinging jet at  $\frac{h}{d} = 4.5$ , NPR 4.0. Dashed squares indicate areas of interest for the coefficients of variation presented in Table 1

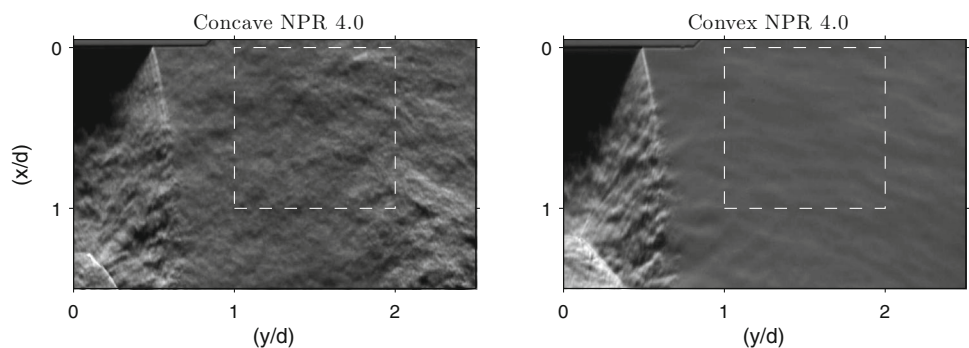


**Fig. 12** Instantaneous schlieren images of underexpanded jets impinging on the convex plate at  $(\frac{h}{d})$  4.5, NPR 3.8 (left) and NPR 4.0 (right)

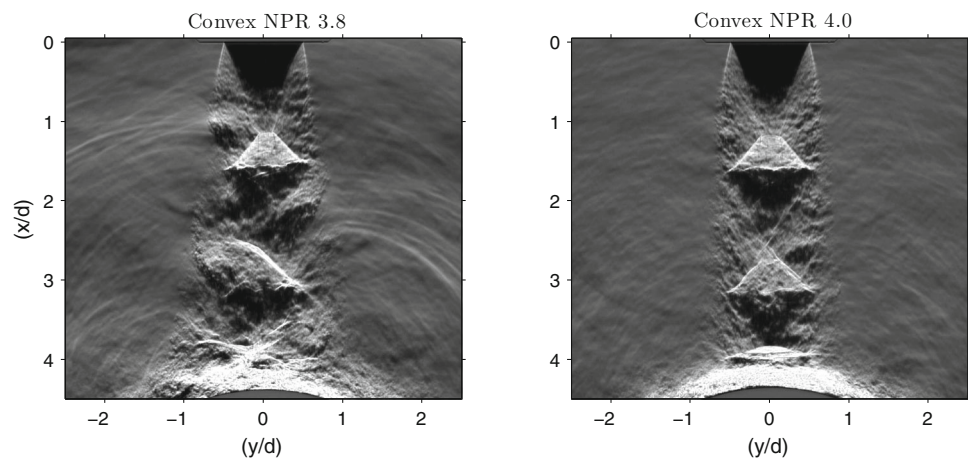


**Table 1** Coefficients of variation for the schlieren region of interest in Fig. 11

	Concave NPR 4.0	Convex NPR 4.0
$(\frac{\sigma}{\mu})_{\text{roi}}$	0.2	0.06

ence and absence of high-amplitude impingement tones are presented in Fig. 12 (left and right, respectively).

The coefficient of variation for the convex case (Table 1) provides a ‘signature’ of the variation resulting from acoustic emission and entrained flow where the wall jet does not recirculate. The significantly greater fluctuation for the concave case reinforces the observation that the wall jet is recirculated and entrained, supporting the proposed mechanism. Though the changes in flow properties that give rise to these changes in density gradient cannot be measured through schlieren, the greater fluctuation for the concave case is indicative of mixing in the recirculating turbulent wall jet. Similar to the effect of nozzle tabs on entrainment and mixing, the concave surface curvature may alter the mixing characteristics of the initial shear layer of the impinging jet. This reduces the jet’s receptivity to acoustic excitation, breaking the feedback loop and suppressing impingement tones.

#### 4 Conclusion

Flow visualisation images and acoustic observations have been used to investigate the impingement of underexpanded jets on to convex and concave half-cylinders. Mean shock structures are asymmetric on the convex plate and a function of the jet pressure ratio. Convex surface curvature constrains flapping jet oscillations to a single plane, the normal of which is parallel to the cylinder axis. Concave cylindrical surface curvature suppresses impingement tone formation, attributable to recirculation of the turbulent wall jet into the entrainment field.

**Acknowledgments** The authors gratefully acknowledge the support given to the project by the Australian Research Council.

#### References

- Alvi, F.S., Lou, H., Shih, C., Kumar, R.: Experimental study of physical mechanisms in the control of supersonic impinging jets using microjets. *J. Fluid Mech.* **613**, 55–83 (2008)
- Carling, J.C., Hunt, B.L.: The near wall jet of a normally impinging, uniform, axisymmetric, supersonic jet. *J. Fluid Mech.* **66**, 159–176 (1974)
- Cornaro, C., Fleischer, A.S., Goldstein, R.J.: Flow visualization of a round jet impinging on cylindrical surfaces. *Exp. Therm. Fluid Sci.* **20**, 66–78 (1999)
- Donaldson, C.D., Snedeker, R.S.: A study of free jet impingement. Part 1. Mean properties of free and impinging jets. *J. Fluid Mech.* **45**, 281–319 (1971)
- Edgington-Mitchell, D., Oberleithner, K., Honnery, D.R., Soria, J.: Coherent structure and sound production in the helical mode of a screeching axisymmetric jet. *J. Fluid Mech.* **748**, 822–847 (2014)
- Henderson, B., Powell, A.: Experiments concerning tones produced by an axisymmetric choked jet impinging on flat plates. *J. Sound Vib.* **168**, 307–326 (1993)
- Henderson, B.: The connection between sound production and jet structure of the supersonic impinging jet. *J. Acoust. Soc. Am.* **111**, 735–747 (2002)
- Henderson, B., Bridges, J., Wernet, M.: An experimental study of the oscillatory flow structure of tone-producing supersonic impinging jets. *J. Fluid Mech.* **542**, 115–137 (2005)
- Jennions, I.K., Hunt, B.L.: The axisymmetric impingement of supersonic air jets on cones. *Aeronaut. Q.* **31**, 26–41 (1980)
- Krothapalli, A., Rajkuperan, E., Alvi, F., Lourenco, L.: Flow field and noise characteristics of a supersonic impinging jet. *J. Fluid Mech.* **392**, 155–181 (1999)
- Kumar, R., Wiley, A., Venkatakrisnan, L., Alvi, F.: Role of coherent structures in supersonic impinging jets. *Phys. Fluids* **25**(7), 076101 (2013)
- Lamont, P.J., Hunt, B.L.: The impingement of underexpanded axisymmetric jets on wedges. *J. Fluid Mech.* **76**, 307–336 (1976)
- Lamont, P.J., Hunt, B.L.: The impingement of underexpanded, axisymmetric jets on perpendicular and inclined flat plates. *J. Fluid Mech.* **100**, 471–511 (1980)
- Mitchell, D.M., Honnery, D.R., Soria, J.: The visualization of the acoustic feedback loop in impinging underexpanded supersonic jet flows using ultra-high frame rate schlieren. *J. Vis.* **15**, 333–341 (2012)

15. Mitchell, D.M., Honnery, D.R., Soria, J.: Near-field structure of underexpanded elliptic jets. *Exp. Fluids* **54**, 1–13 (2013)
16. Powell, A.: The sound-producing oscillations of round underexpanded jets impinging on normal plates. *J. Acoust. Soc. Am.* **83**, 515–533 (1988)
17. Powell, A.: Lord Rayleigh's foundations of aeroacoustics. *J. Acoust. Soc. Am.* **98**, 1839–1844 (1995)
18. Reeder, M.F., Samimy, M.: The evolution of a jet with vortex-generating tabs: real-time visualization and quantitative measurements. *J. Fluid Mech.* **311**, 73–118 (1996)
19. Risborg, A., Soria, J.: High-speed optical measurements of an underexpanded supersonic jet impinging on an inclined plate. In: Kleine, H., Guillén, M.P.B. (Eds.) 28th International Congress on High-speed Imaging and Photonics, Proc. SPIE, vol. 7126, pp. F-1–F-11 (2009)
20. Tam, C.K.W., Ahuja, K.K.: Theoretical model of discrete tone generation by impinging jets. *J. Fluid Mech.* **214**, 67–87 (1990)
21. Tam, C.K.W.: Supersonic jet noise. *Annu. Rev. Fluid Mech.* **27**, 17–43 (1995)
22. Willert, C.E., Mitchell, D.M., Soria, J.: An assessment of high-power light-emitting diodes for high frame rate schlieren imaging. *Exp. Fluids* **53**, 413–421 (2012)